

Learning Objectives

- To know MR techniques useful to quantify liver steatosis, iron overload, and fibrosis.
- To learn about less common liver storage diseases.
- Discuss the MR imaging appearance of focal lesions in the cirrhotic liver and the use of the standardized reporting system LI-RADS.
- Learn about diffuse vascular liver disease causing liver parenchyma alteration.

6.1 Metabolic and Storage Diseases

6.1.1 Steatosis

Non-alcoholic fatty liver disease (NAFLD) represents a global epidemic which is now estimated to affect up to 25% of the world's adult population. Approximately 1 in 5 patients with NAFLD will develop non-alcoholic steatohepatitis (NASH), soon expected to overtake viral hepatitis as the leading cause of cirrhosis worldwide [1]. Non-invasive assessment of NAFLD is therefore of increasing importance given the limitations and risks associated with liver biopsy, in order to enable the diagnosis and monitoring of affected individuals. Although unenhanced computed tomography (CT) may allow the identification of individuals with moderate to severe steatosis, a threshold of 48 Hounsfield Units (HU) being highly specific for its

detection, given the associated radiation burden it is an impractical modality for large-scale monitoring and may be confounded by the co-existence of other materials such as iron [2] (Fig. 6.1). However, advances in magnetic resonance imaging (MRI) have enabled a more comprehensive assessment of steatosis. The most widely utilized technique is that of dual gradient-echo imaging, in which images are acquired with fat and water proton signals being either “in-phase” or “out-of-phase,” the latter usually being acquired first. Voxels containing both fat and water appear relatively hypointense in the “out-of-phase” images due to signal cancellation, a result of the differing precession frequencies of fat and water protons, thereby enabling the identification of either diffuse or geographic steatosis within the parenchyma (Fig. 6.2).

However, while this may be a useful technique for the subjective assessment of steatosis, multiple confounding factors—including T2* decay, of particular importance if iron overload is present—limit its use for the reliable quanti-

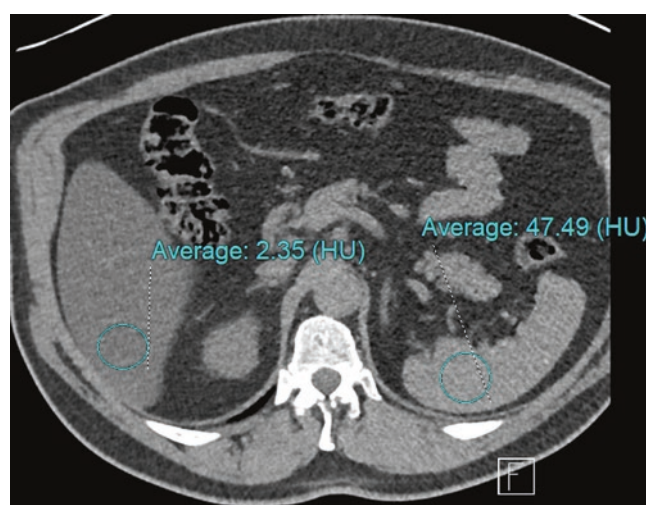


Fig. 6.1 Unenhanced CT image of severe steatosis demonstrating hepatic attenuation more than 10HU less than the spleen, and far below the proposed threshold of 48HU for moderate-severe steatosis

D. Bowden
Department of Radiology, Cambridge University Hospitals,
Cambridge, UK

C. S. Reiner (✉)
Institute of Diagnostic and Interventional Radiology,
University Hospital Zurich, Zurich, Switzerland
e-mail: caecilia.reiner@usz.ch

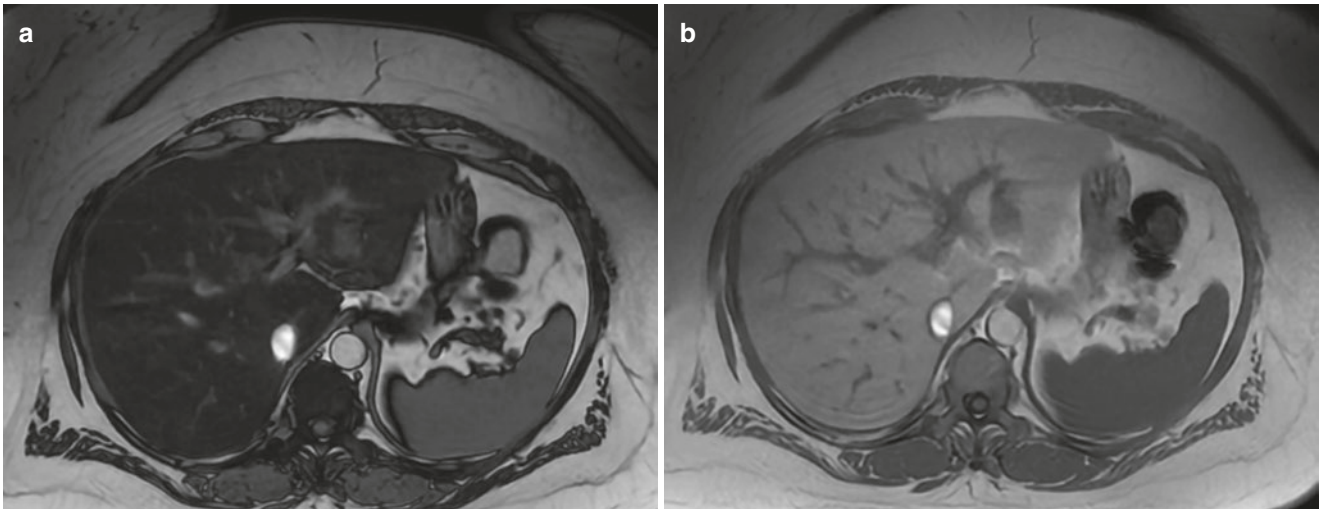


Fig. 6.2 Dual gradient-echo T1-weighted images of severe steatosis. (a) Out-of-phase image demonstrating marked liver parenchymal signal drop when compared with the in-phase image (b)

fication of fat and have led to the development of more complex sequences which account for these factors. Each major MR vendor has developed variations of a rapid breath-hold multi-echo technique which enables the measurement of the proton density fat fraction (PDFF)—defined as the fraction of mobile triglyceride protons relative to those of water (IDEAL IQ/GE, mDixon-Quant/Philips, and Multiecho VIBE Dixon/Siemens). Using a derived map, measurement of PDFF values is as simple as drawing an ROI within the parenchyma, allowing for variations in fat distribution, with proposed intervals for histological steatosis grading being grade 0 (normal, 0–6.4%), grade 1 (mild, 6.5–17.4%), grade 2 (moderate, 17.5–22.1%), and grade 3 (severe, 22.2% or greater)—Fig. 6.3. PDFF values using this technique have been well validated as a biomarker of steatosis, including when compared with histopathological and MR spectroscopy results [3].

6.1.2 Iron Overload

Due to the formation of free radicals, excess iron accumulation within body tissues is toxic and may result in organ damage—in particular to the liver, heart, and pancreas. It arises most commonly from either excessive intestinal absorption (e.g., hereditary hemochromatosis, iron supplementation) or chronic blood transfusions (e.g., patients with hemoglobinopathies or other red cell disorders). In the case of the latter, a form of hemosiderosis, iron accumulates predominantly within the reticuloendothelial system of the liver and other organs and while its measurement is required as part of the monitoring of therapy, is less damaging to the liver than to other organs such as the heart. As a result of abnormal metabolism, the presence of chronic liver disease

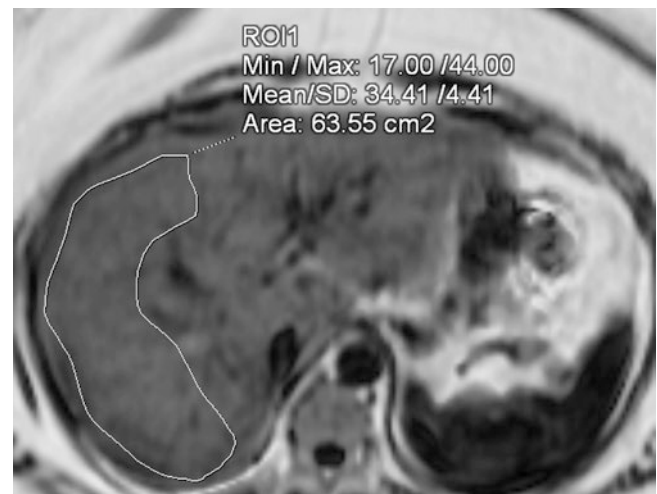


Fig. 6.3 Severe steatosis. Proton density fat fraction (PDFF) map derived using the multi-echo IDEAL IQ (GE) technique. ROI placement avoiding major vessels provides a simple percentage of fat within the parenchyma, in this case 34%

in itself, arising from NAFLD, alcohol-related liver disease or other causes, may also lead to iron accumulation which can further accelerate disease progression [4]. Evaluation of hepatic iron is therefore of importance in both the diagnosis and monitoring of patients at risk of iron overload.

While liver biopsy has historically represented the gold standard for its assessment, non-invasive methods such as MRI which are also less prone to sampling error are desirable. In addition, iron may not be distributed evenly throughout the liver parenchyma and pathological methods used in its precise quantification result in the destruction of specimens, precluding histological analysis. The presence of iron particles within tissues results in tiny inhomogeneities

within the magnetic field, leading to rapid dephasing of protons, shortening of T1, T2, and T2* relaxation times and therefore an increase in R2*, the rate of T2* relaxation. During the acquisition of dual gradient-echo images as previously described, signal loss is therefore visible in the second, in-phase acquisition and a qualitative assessment of iron overload is possible (Fig. 6.4). The presence of concomitant steatosis, which results in signal loss in the first (out-of-phase) image, will however confound the appearance and more sophisticated techniques are required for formal quantification. While a full review is beyond the scope of this chapter, techniques such as those already described for steatosis quantification also allow the calculation of iron content. Multipoint Dixon techniques such as IDEAL-IQ (GE) not only provide a PDFF map in a single breath hold,

but also a simultaneous R2* map upon which ROIs can be placed to calculate mean R2* values for the liver parenchyma (Fig. 6.4). These values are then converted to a Liver Iron Concentration (LIC) value using a simple calibration formula. While it is unconfirmed which of several calibration formulae is most appropriate, evidence suggests differences between the results are small and for practical purposes any may be used [5]. Alternatively, spin echo techniques such as R2 relaxometry (e.g., Ferriscan®, Resonance Health) are also available and show excellent correlation with LIC values, but have the disadvantages of additional cost, long (up to 20 min) acquisition times that limit its use in difficult patients, off-site centralized analysis, and the lack of radiologist input to scrutinize images for significant findings such as HCC.

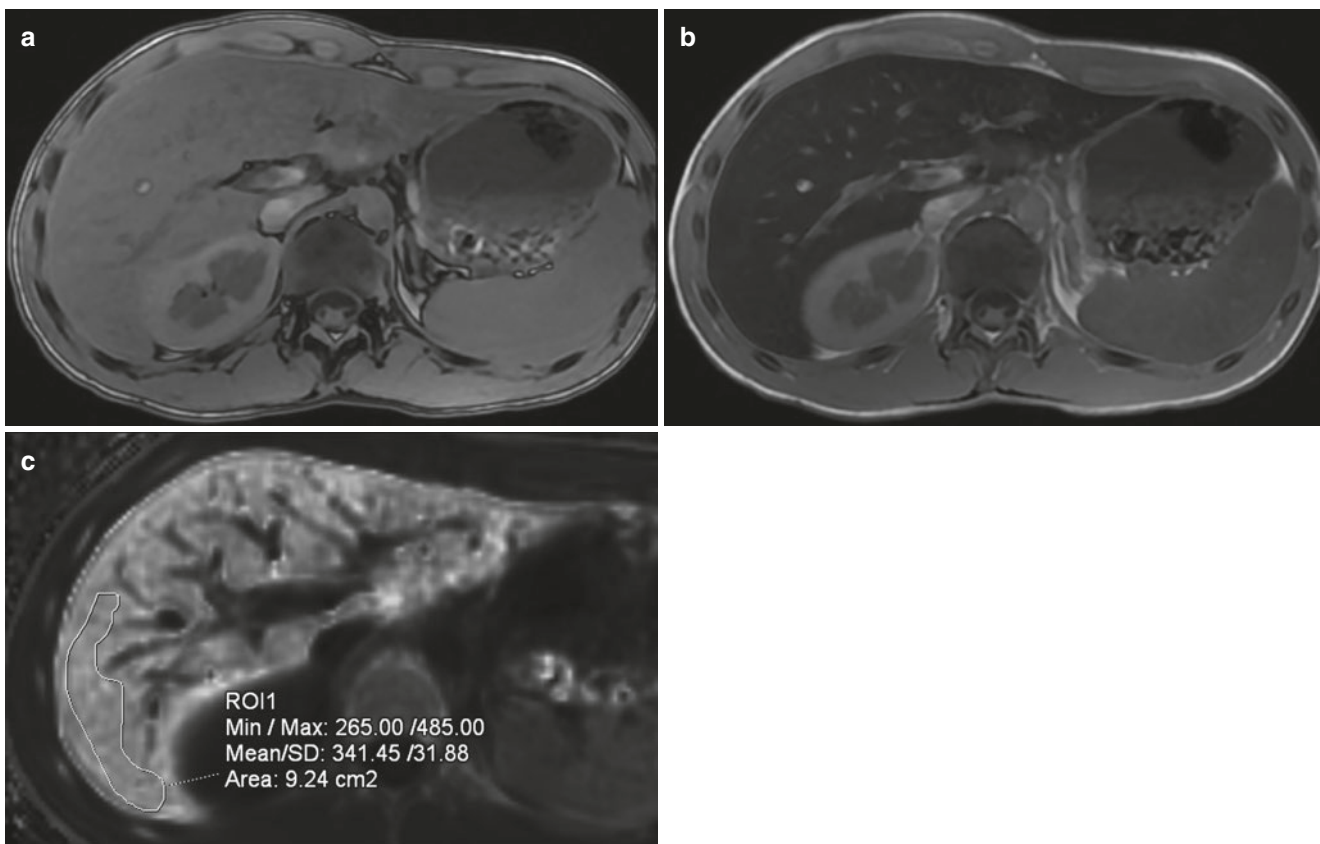


Fig. 6.4 Hepatic and splenic iron overload. Dual gradient-echo images of iron deposition in a patient who has received multiple blood transfusions. (a) Out-of-phase, (b) in-phase images. Due to dephasing of protons as a result of magnetic field inhomogeneity in the presence of iron, signal drop occurs within the liver parenchyma between the first (out-of-phase) and second (in-phase) echoes. Similar change is seen within the spleen as a result of iron deposition within the reticuloendothelial

system following chronic transfusions. (c) Formal measurement of liver iron concentration. ROI placement on the R2* map derived using the multi-echo IDEAL IQ (GE) technique allows for liver iron concentration measurement, following conversion using a calibration formula. In this case, the R2* value = 341 s^{-1} (Normal $<67 \text{ s}^{-1}$ at 1.5 T), equivalent to 8.9 mg Fe/g dry liver (normal $<1.8 \text{ mg Fe/g}$)—equivalent to severe overload

Key Points

For both iron and fat quantification, MR techniques have proven the most robust and include multi-echo single breath-hold acquisitions, available via each MR vendor, which unlike CT and MR are able to account for confounding variables. Given the rising epidemic of NAFLD, their inclusion as standard in liver imaging protocols is to be encouraged.

6.1.3 Wilson's Disease

Wilson's disease, or progressive hepatolenticular degeneration, is a rare autosomal recessive disorder of metabolism in which copper accumulates in multiple organs, in particular within the liver but also within the brain, kidney, and cornea. As a result, a spectrum of pathophysiologic changes occurs including steatosis, chronic active hepatitis and ultimately, cirrhosis. Imaging findings are somewhat non-specific and overlap significantly with chronic liver disease of other etiologies. These include an irregular capsular contour, T2 hypo/T1 hyperintense nodules and parenchymal heterogeneity with increased echogenicity at ultrasound. It has however been suggested that a relative lack of caudate lobe hypertrophy may be a more specific feature [6].

6.1.4 Amyloidosis

Amyloidosis refers to a spectrum of diseases in which extracellular accumulation of the fibrillar protein amyloid occurs, which may be either focal or diffuse and may involve several organs or be limited to one. Its most common forms are the AL type (amyloid light chain, formerly known as primary amyloidosis), associated with plasma cell dyscrasias, or AA type (amyloid A, formerly secondary amyloidosis) arising from systemic inflammation. Infiltration within the liver occurs predominantly along the sinusoids and results in the non-specific signs of hepatomegaly, increased echogenicity

at US with hypoattenuation at CT mimicking steatosis and heterogeneous enhancement following contrast medium administration. Elastography demonstrates increased hepatic stiffness which may be heterogeneous, diffuse or more focal and may therefore have a role in assessment of affected patients for liver involvement [7].

Key Points

Wilson's disease and amyloidosis have non-specific imaging findings which overlap significantly with other etiologies of liver disease although in the correct clinical context MR Elastography may show promise in the identification of liver involvement with amyloidosis.

6.1.5 Gaucher Disease

Gaucher disease is a rare lysosomal storage disorder in which a cell membrane glycosphingolipid accumulates within reticuloendothelial macrophages ("Gaucher cells") due to a hereditary deficiency in the GBA1 enzyme. Of the three types, type 1 is the most common in which Gaucher cells accumulate within the liver, spleen, and bone marrow and result in several clinical manifestations such as anemia, hepatosplenomegaly, and avascular necrosis of bone. Since the advent of enzyme replacement therapy, MRI has played a key role in the monitoring of response to treatment, both via the volumetric analysis of the liver and spleen as well as evaluation for malignancy. Gaucher disease may result in cirrhosis and is associated with an increased risk of solid organ malignancy, including HCC, in the context of both cirrhotic and non-cirrhotic livers [8]. Differentiation of HCC from benign entities such as focal nodular hyperplasia may be very challenging given the overlap in imaging features. In addition, focal accumulation of Gaucher cells within the liver and spleen may result in the so-called Gaucheromas, nodules which have highly variable imaging appearances, and which are a diagnosis of exclusion (Fig. 6.5).

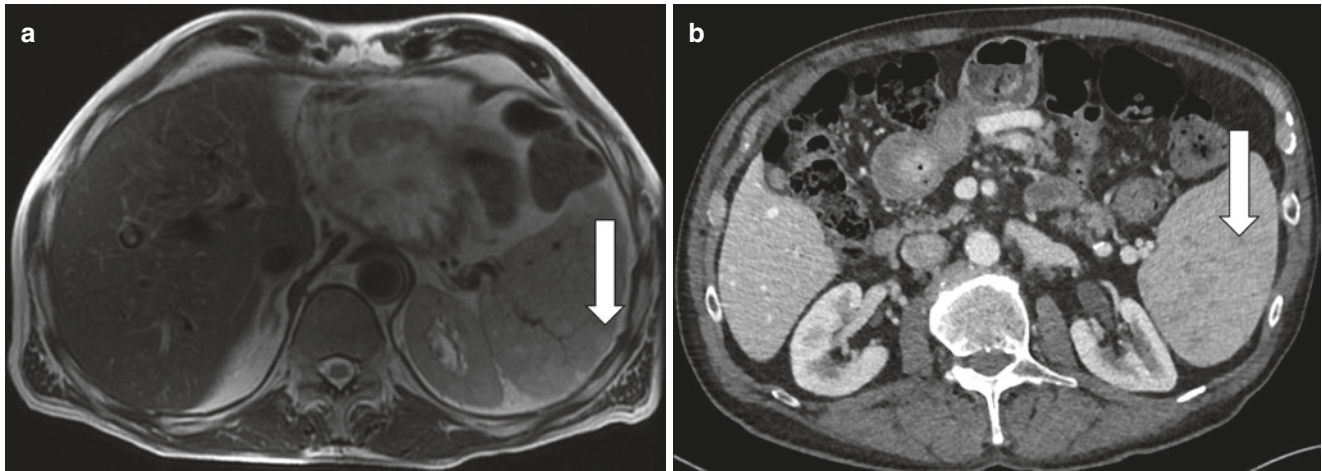


Fig. 6.5 (a, b) Gaucheromas within the spleen. (a) Axial T2-weighted image demonstrates multiple well-defined T2 hyperintense lesions (arrow), which appear relatively hypoenhancing in portal venous phase CT (b)

6.2 Cirrhosis

6.2.1 Imaging of Pre-stages of Cirrhosis

Regardless of etiology, chronic liver injury leads to inflammation and hepatocellular damage with resultant fibrosis and regeneration of hepatocytes. Stage 4 fibrosis, or cirrhosis, represents the end stage of this process and as described previously, Hepatitis B, C and alcohol-related liver disease are likely to be soon overtaken by NAFLD as its leading cause. Early detection and monitoring of fibrosis is therefore of critical importance. Although previously liver biopsy has been regarded as the gold standard for its evaluation, non-invasive techniques are desirable given the risks associated with biopsy and sampling error, fibrosis frequently having a heterogeneous distribution. While ultrasound techniques such as transient elastography (Fibroscan[®]) or 2D shear wave elastography are readily available, performance is poor in the presence of ascites or obesity and such techniques are also limited by small sample size and operator factors.

MR elastography has emerged as the most accurate technique for the non-invasive detection and staging of fibrosis, enables sampling of the entire liver, including in the presence of obesity and ascites, and is able to provide additional information on the geographic distribution of fibrosis [9]. Low frequency acoustic waves are transmitted through the

abdominal wall overlying the liver using an acoustic driver, resulting in shear wave propagation through the parenchyma. Using a 2D gradient-echo sequence, 60 Hz motion-encoding gradients are synchronized to the driver motion in order to acquire images of propagating waves; magnitude and phase images are then used to derive a stiffness map at four adjacent slice locations, each in a single breath hold (Fig. 6.6). During post-processing, a confidence map is overlaid on the map to exclude unreliable data. The reader then draws an ROI on the confidence map, excluding large vessels, the liver edge, perihepatic tissues/fissures, and artifacts. A weighted mean of values derived from the four slices is then calculated to provide overall liver stiffness. While stiffness values have a relatively narrow range for each stage of fibrosis, its accuracy for both “ruling in” the presence of significant fibrosis and “ruling out” cirrhosis is excellent [10]. Drawbacks include the need for meticulous technique—in particular driver placement and slice location—and the presence of iron, which results in signal loss. While spin echo techniques may mitigate the latter if mild, commercial availability is limited and more severe cases of iron overload will still result in failure (Fig. 6.7). Further pitfalls include the presence of biliary obstruction, inflammation, or congestion due to right-sided heart failure, all of which may increase hepatic stiffness. Results therefore always require interpretation in the overall clinical context.

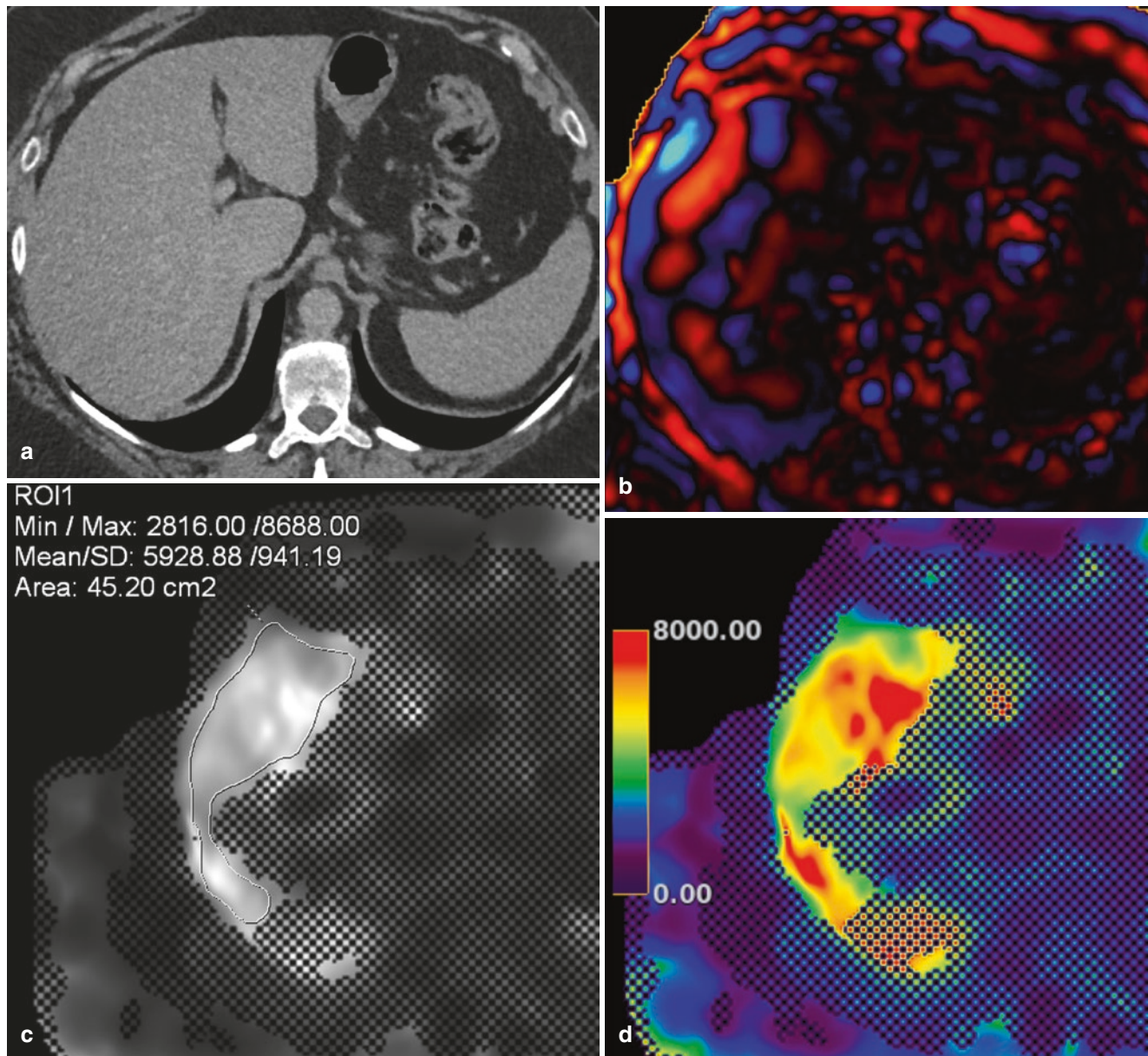


Fig. 6.6 MR Elastography of cirrhosis in a patient with normal liver morphology. (a) Portal venous phase CT image demonstrates a relatively normal morphology, with a lack of capsular irregularity, lobar atrophy/hypertrophy, or splenomegaly. (b) MRE wave image, required to inspect data quality. (c) Grey-scale elastogram: ROI placement

avoiding the liver edge and major vessels allows measurement of hepatic stiffness in pascals, in this case 5.9 kPa (>5.0 kPa = stage 4 fibrosis/cirrhosis). (d) Color elastogram, used to analyze the distribution of hepatic stiffness which in some cases may provide additional information regarding etiology. Scale is in Pascals

6.2.2 Imaging of Cirrhosis

Cirrhosis is the result of chronic damage to the liver, characterized by progressive fibrosis of the liver parenchyma with ongoing regeneration. Beside the etiologies of cirrhosis described above other causes are hemochromatosis or biliary and cryptogenic diseases. On imaging, the liver may appear normal at an early stage of cirrhosis. With disease progression, heterogeneity and surface nodularity are observed. Because of the unique ability of the liver to regenerate in

cirrhosis, the liver harbors a spectrum of hepatocellular nodules, most of which are regenerative. Due to the ongoing distortion of the liver parenchyma, the liver surface appears nodular, or lobular in most of the cases. Caudate lobe hypertrophy is the most characteristic morphologic feature of liver cirrhosis [11]. Alteration of blood flow results in typical morphologic abnormalities: segmental hypertrophy involving the lateral segments of the left lobe (segment 2, 3), and segmental atrophy affecting the right lobe (segment 6, 7) and medial segment of the left lobe (segment 4). Other typical

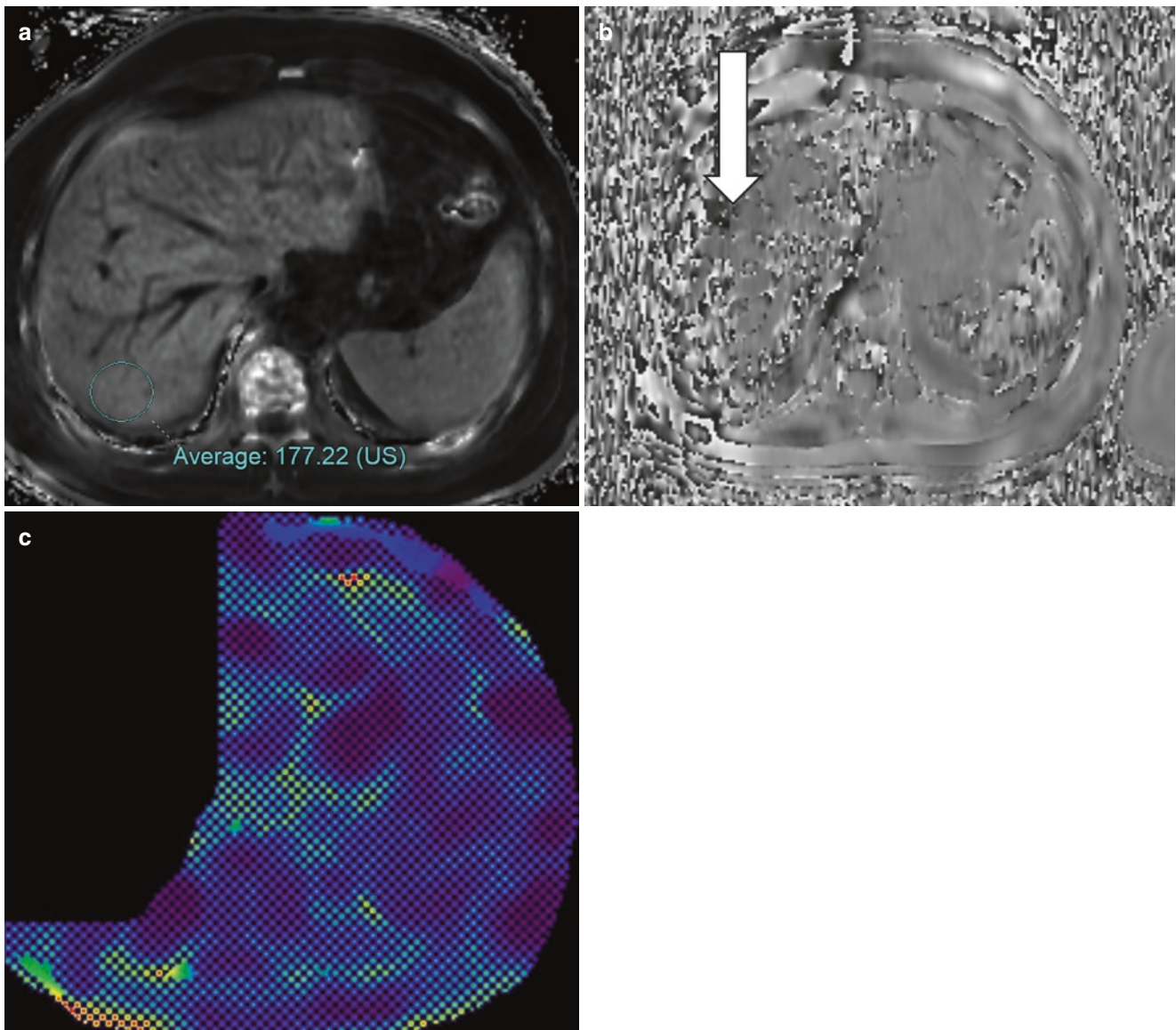


Fig. 6.7 Failure of MRE in a patient with iron overload. (a) $R2^*$ map derived from IDEAL IQ (GE) acquisition demonstrates an $R2^*$ value of 177 s^{-1} , equating to a liver iron concentration of $= 4.7 \text{ mg Fe/g dry}$

weight (DW), moderate iron overload (normal $<1.8 \text{ mg/g DW}$). (b) Phase image shows diffuse signal loss within the liver parenchyma, visible in the color elastogram (c) as a signal void

findings include enlargement of hilar periportal space, the right posterior notch-sign and generalized widening of the interlobar fissures. Less typical distribution of segmental atrophy and hypertrophy is seen in primary sclerosing cholangitis, where the distribution follows in part the distribution of the bile duct involvement, for example, atrophy of segments 2 and 3 or 5 and 7 may be seen. The segmental compensatory hypertrophy associated with atrophy of other liver parts may appear as pseudotumoral enlargement. In 25% of cirrhosis, the liver shape and contour appear normal on CT or MRI.

Lymphadenopathy can appear in the liver hilum and peripancreatic region, which may mimic neoplastic lymph

nodes, if the lymph nodes are large. Portal hypertension due to increased vascular resistance at the level of the hepatic sinusoids causes complications such as ascites, development of portosystemic shunts at the distal esophagus and the gastric fundus, via periumbilical veins and left gastric vein. Other shunts include splenorenal collaterals, hemorrhoidal veins, abdominal wall, and retroperitoneal collaterals [11]. These collateral veins are seen as enhancing tortuous vessels. The typical nodular liver contour and liver shape of cirrhosis as well as its vascular complications can be seen on ultrasound, CT, or MRI. MRI very well depicts fibrotic bands between regenerative nodules as T2 hyperintense and progressively or delayed enhancing structures.

Key Points

MR elastography has emerged as the most accurate technique for the detection and staging of hepatic fibrosis and cirrhosis.

6.3 Focal Lesions in Cirrhotic Liver

6.3.1 Regenerative Nodules

Regenerative nodules in a cirrhotic liver play a role in the stepwise carcinogenesis of HCC, most frequently through dedifferentiation from regenerative nodule, low-grade dysplastic nodule, high-grade dysplastic nodule to HCC. Most regenerative nodules do not progress in the dedifferentiation process. They are macronodular (≥ 9 mm) or micronodular (3–9 mm). Most regenerative nodules are not seen as distinct nodules on CT or MRI, but rather as nodular appearance of the liver parenchyma. MRI detects regenerative nodules with a higher sensitivity than US or CT. Regenerative nodules are usually iso- to hypointense on T2-weighted images and isointense on T1-weighted images. Variable signal intensity on T1-weighted images is due to lipid, protein, or copper content leading to a T1-weighted hyperintense appearance or iron deposition in the so-called siderotic nodules with a hypointense appearance on T1-weighted and T2-weighted images. Using extracellular gadolinium-containing contrast agent, regenerative nodules show the same contrast behavior as the background liver. After administration of hepatocyte-specific contrast material regenerative nodules usually enhance to the same degree as adjacent liver [12]. Some regenerative nodules—the so-called focal nodular hyperplasia like nodules—may also show arterial enhancement and increased uptake of hepatocyte-specific contrast agent compared to the surrounding liver, which may make them difficult to differentiate from hepatocellular carcinoma [13].

6.3.2 Dysplastic Nodules

Dysplastic nodules are regenerative nodules that contain atypical hepatocytes, measuring at least 1 mm, not meeting histologic criteria for malignancy. They are classified as low- or high-grade dysplastic nodules. High-grade dysplastic nodules are considered premalignant. The differentiation between a regenerative nodule and a low-grade dysplastic nodule is difficult due to similar appearance on MRI. Dysplastic nodules are rarely detected on CT. Dysplastic nodules usually are

hypovascular. In high-grade dysplastic nodules, arterial vascularization can increase leading to arterial hyperenhancement on imaging. Using hepatocyte-specific MR contrast agents, dysplastic nodules show variable signal intensity in the hepatocyte-specific phase. With progressing dedifferentiation, the nodules lose their ability to take up the hepatocyte-specific contrast agent and appear hypointense in the hepatobiliary phase. These hepatobiliary hypointense dysplastic nodules may be mistaken for HCC. Dysplastic nodules may also instead lose the ability to excrete the hepatocyte-specific contrast agent and appear iso- or hyperintense on hepatobiliary phase images. Hypovascular cirrhotic nodules with hypointense appearance in the hepatobiliary phase carry a significant risk of transforming into hypervascular HCC with a pooled overall rate of 28% (95% CI, 22.7–33.6%). The size of the hypovascular nodule is a second risk factor for hypervascular transformation with nodules ≥ 9 mm in size showing a higher risk [14].

6.3.3 Malignant Lesions

Hepatocellular carcinoma (HCC) occurs as a solitary lesion (in half of the cases), as multiple lesions or diffuse. The vast majority of HCCs (90%) occur in cirrhotic livers. In this setting, HCCs can be commonly diagnosed based on imaging features alone without histological confirmation [15]. The second most common primary hepatic tumor is intrahepatic cholangiocarcinoma (ICC), which accounts for 10–20% of all primary hepatic tumors. Recently, cirrhosis and viral hepatitis C and B have been recognized as risk factors for cholangiocarcinoma, especially for the intrahepatic type [16]. Radiologic features of cholangiocarcinoma such as progressive contrast enhancement from arterial to venous and late phase, arterial rim enhancement, and peripheral washout can help differentiate ICC from HCC in the cirrhotic liver [17]. The imaging characteristics of focal HCC and ICC are discussed in the chapter on “Focal liver lesions.”

A challenging diagnosis is the diagnosis of diffuse HCC, or also known as infiltrative HCC in a cirrhotic liver, which accounts for 7–20% of HCC cases. Diffuse HCC usually spreads over multiple liver segments and is frequently associated with portal vein tumor thrombosis. The tumor is often difficult to distinguish from background changes in cirrhosis at imaging and portal vein thrombosis may be the only obvious finding. The tumor often shows only minimal arterial enhancement and heterogeneous washout on contrast-enhanced CT or MRI. Diffusion-weighted MRI can be helpful as the tumor appears hyperintense compared to the cirrhotic liver [18].

6.3.4 Confluent Focal Fibrosis

In advanced stages of cirrhosis additional focal fibrosis can appear as wedge-shaped area from the porta hepatis to the liver surface. This so-called confluent focal fibrosis is typically located in segments 4, 7, or 8, leads to capsular retraction, and appears as hypointense area on T1-weighted MRI. It is slightly hyperintense on T2, shows late enhancement with extracellular contrast agents due to contrast accumulation in fibrotic tissue and hepatobiliary phase hypointensity (Fig. 6.8) [19].

6.3.5 Standardized Reporting with LI-RADS

Due to a great overlap in imaging features across the spectrum of cirrhotic nodules from regenerative nodules to poorly differentiated HCC, a definite diagnosis of a benign or malignant lesion is often not possible. Furthermore, a great variety

in nomenclature of imaging features of cirrhotic nodules is used. To overcome these difficulties, the Liver Imaging-Reporting and Data System (LI-RADS) has been developed, which is a comprehensive system for standardized interpretation and reporting of computed tomography (CT) and magnetic resonance (MR) examinations performed in patients at risk for HCC. It uses a standardized nomenclature and provides a diagnostic algorithm that uses imaging features to categorize the observations seen in patients at risk for HCC along a spectrum from benign to malignant. Liver lesions in these patients are rated for their risk of being an HCC. LI-RADS 1 category observations demonstrate imaging features diagnostic of a benign entity, for example, cyst and hemangioma. LI-RADS 2 observations are probably benign, such as a hemangioma with an atypical enhancement pattern or a probably benign cirrhotic nodule. Major features including arterial-phase enhancement, lesion diameter, washout appearance, capsule appearance, and threshold growth are imaging features used to categorize LI-RADS 3

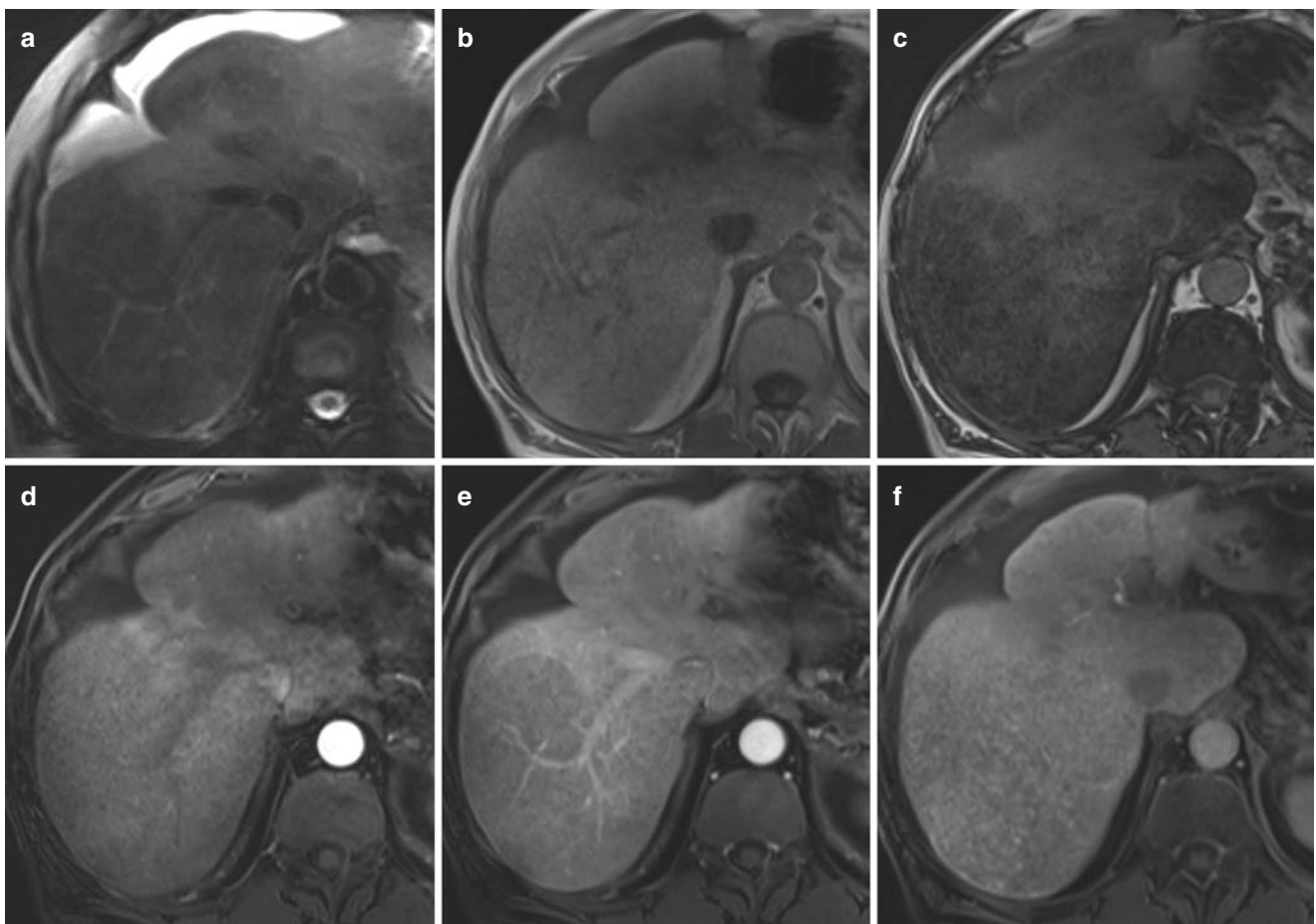


Fig. 6.8 Confluent focal fibrosis. A 62-year-old man with cirrhosis. (a) Axial T2-weighted fat saturated image with capsular retraction in liver segment VIII and adjacent focal hyperintense area. The liver parenchyma shows signal drop from in-phase (b) to opposed-phase (c)

images corresponding to diffuse fat deposition with exception of the area in segment VIII. The area of focal fibrosis in segment VIII shows slight arterial (d) and portal venous (e) enhancement and subtle hypointensity in hepatobiliary phase (f)

(indeterminate probability of HCC), LI-RADS 4 (probably HCC), and LI-RADS 5 (definitely HCC) lesions. LI-RADS 5 lesions have typical imaging features diagnostic for HCC. To further refine and adjust LI-RADS categories ancillary imaging features favoring benignity or malignancy can be used [20].

Key Points

Regenerative and dysplastic nodules share overlapping imaging features and may be difficult to distinguish. LI-RADS helps in rating the risk of such a focal lesion in cirrhosis of being an HCC.

6.4 Diffuse Vascular Liver Disease

6.4.1 Arteriovenous Shunts

Intrahepatic arterioportal shunts are communications between the hepatic arterial system and a portal vein or between hepatic arteries and hepatic veins which can be either at the level of the trunk, sinusoids, or peribiliary venules. In a cirrhotic liver, they can occur spontaneously, represent pseudolesions and subsequently resolve. Secondary shunts may be posttraumatic, post biopsy, or instrumentation. On imaging, they appear as small, peripheral, nonspherical enhancing foci, which become isoattenuating to the liver in the portal venous phase. It may be difficult to distinguish an arterioportal shunt from a small hepatocellular carcinoma. Repeating imaging after 6 months usually helps distinguishing, these entities and demonstrates resolution or stability of an arterioportal shunt, or growth of an HCC.

6.4.2 Budd-Chiari Syndrome

Budd-Chiari syndrome is defined as lobar or segmental hepatic venous outflow obstruction at the level of the inferior vena cava (IVC, type 1), at the level of the hepatic veins (type 2) or occlusion of small centrilobular veins (type 3). The most common cause of hepatic vein obstruction is thrombosis, most commonly due to hypercoagulability (oral contraceptive use, pregnancy, polycythemia) or less common due to obstruction after chemotherapy or radiation. Other primary causes are webs and membranes in the hepatic veins or IVC either of congenital origin or after thrombosis. The outflow obstruction may also be due to extrinsic compression of the hepatic outflow by hepatic masses (malignant or non-malignant). The imaging findings in the acute phase differ from the chronic

phase. In the acute state, the inferior vena cava (IVC) and/or hepatic veins may appear hyperattenuating on unenhanced CT images because of the increased attenuation of a thrombus. On contrast-enhanced CT or MRI a vascular filling defect due to thrombotic material, reduction of hepatic vein caliber, missing connection between hepatic veins and IVC can be present or hepatic veins may not be visible at all. In the acute phase, hepatomegaly with diminished enhancement of the liver periphery and accentuated enhancement of central liver parts and caudate lobe is seen. Later on, peripheral liver enhancement becomes heterogeneous as disorganized, comma-shaped intrahepatic collateral veins, and systemic collateral veins develop. In chronic Budd-Chiari syndrome, fibrotic changes appear in the liver. Large regenerative nodules in a dysmorphic liver are frequent findings in longer standing venous outflow obstruction. These regenerative nodules appear hyperintense on hepatobiliary phase images after administration of a hepatocyte-specific contrast agent. Hypertrophy of the caudate lobe with variation in attenuation due to separate venous drainage should not be interpreted as a tumor [21]. In chronic Budd-Chiari syndrome not only benign regenerative nodules, but also HCC can develop, which may be difficult to differentiate since both can appear markedly hyperenhanced on arterial phase.

6.4.3 Sinusoidal Obstruction Syndrome

Hepatic sinusoidal obstruction syndrome (SOS) formerly known as “veno-occlusive disease” is characterized by a hepatic venous outflow obstruction in the intrahepatic sinusoidal venules. An injury to the hepatic venous endothelium leads to necrosis and obstruction of sinusoidal venules. SOS can present with severe complications, such as congestive hepatopathy, portal hypertension, impaired liver function, and acute liver failure, but can also remain asymptomatic. SOS can occur in the setting of hematopoietic stem cell transplantation and with different chemotherapeutic agents (mainly oxaliplatin-containing chemotherapies). An association of SOS with herbal remedies containing pyrrolizidine and nonpyrrolizidine alkaloids, consumption of bush tea, and oral contraceptives in women with antiphospholipid syndrome has been described. On CT and MR imaging heterogeneous, mosaic-like enhancement of the liver parenchyma usually located in the periphery of the right lobe is seen. On hepatobiliary phase MR images, liver parenchyma shows varying degrees of reticular hypointensities (Fig. 6.9), which is highly specific for SOS [22]. Indirect signs of severe SOS related to reduced liver outflow and portal hypertension include hepatomegaly, gallbladder wall thickening, peripor-

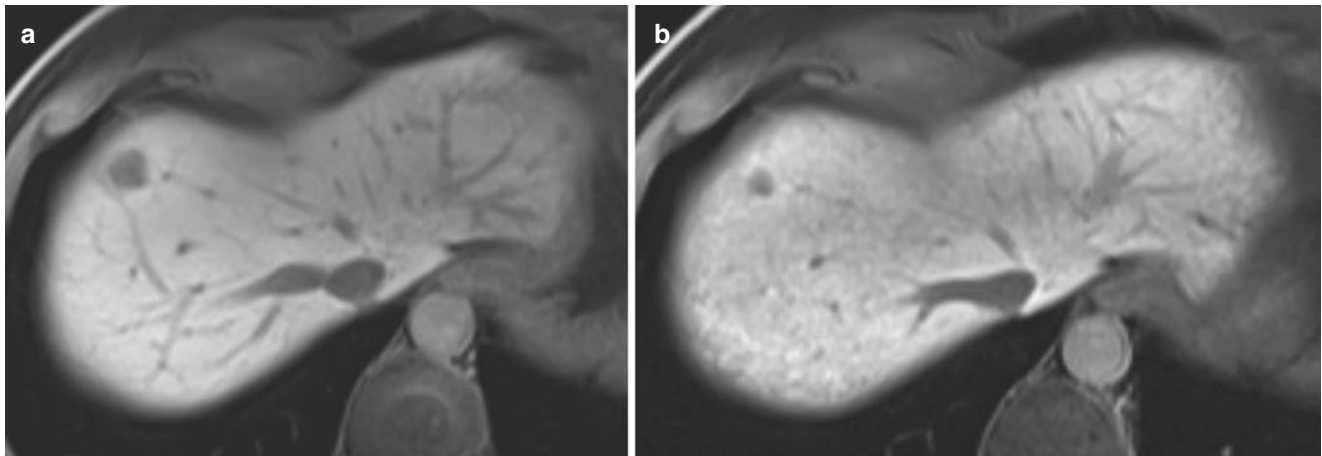


Fig. 6.9 Sinusoidal obstruction syndrome. A 62-year-old man with colorectal liver metastases. (a) Prior to chemotherapy axial hepatobiliary phase image shows a liver metastasis in segment VIII and homogeneous enhancement of the liver parenchyma. (b) After four cycles of

capecitabine and oxaliplatin, the liver metastasis decreased in size. The liver parenchyma shows a reticular hypointense pattern on hepatobiliary phase corresponding to parenchymal changes due to sinusoidal obstruction syndrome

tal edema, splenomegaly, esophageal varices, umbilical vein patency, and ascites [23].

6.4.4 Passive Hepatic Congestion and Fontan-Associated Liver Disease

Passive hepatic congestion is due to chronic right-sided heart failure, which leads to stasis of blood within the liver parenchyma. An enlarged, heterogeneous liver may be seen as a manifestation of acute or early cardiac disease. Early arterial enhancement of the dilated IVC and central hepatic veins is caused by reflux of contrast material from the right atrium into the IVC. A heterogeneous, mottled mosaic pattern of enhancement is present in the parenchymal phase, a condition also known as “nutmeg” liver. In long standing disease, progressive cellular necrosis results in a small cirrhotic liver. Early changes of hepatic congestion are visible on MR Elastography, with a pattern of peripheral T2 hyperintensity (oedema) associated with matching raised parenchymal stiffness. An important patient group in whom this may be seen is those with the so-called Fontan circulation following correction of pediatric congenital heart disease in those born with a single ventricle physiology. As life expectancy has improved, an increasing number of adult patients are now seen in whom chronic hepatic congestion results in the early onset of fibrosis and cirrhosis—Fontan-Associated Liver Disease (FALD). While differentiation of fibrosis and congestion may be difficult or impossible in many cases, and often co-exist, typical patterns of elevated stiffness may provide a clue to the predominant etiology and facilitate appropriate treatment (Fig. 6.10) [24].

6.4.5 Hereditary Hemorrhagic Telangiectasia (HHT)

HHT is an autosomal dominant disorder characterized by vascular malformations (VM) in multiple organs, including the hepatobiliary and gastrointestinal tract. VMs occur in up to 74% of patients with HHT, increase in frequency with age and range from small telangiectasias (dilatation of postcapillary venules that communicate directly with arterioles) to larger shunts between arteries and hepatic or portal veins, as well as between portal and hepatic venous branches [25]. In severe cases, these may lead to significant shunting, portal hypertension, biliary ischemia, high output cardiac failure or hepatic encephalopathy. Dilatation of the common hepatic artery of more than 7 mm is frequently seen, as well as an increased incidence of visceral aneurysms (Fig. 6.11). The so-called confluent vascular masses may arise within the liver parenchyma from the fusion of multiple smaller telangiectasias, in addition to large regenerative nodules and focal nodular hyperplasia (FNH), the latter demonstrating typical arterial hyperenhancement with retention of hepatobiliary contrast agents in the delayed phase.

Key Points

Vascular disorders of the liver may be either congenital (e.g., HHT) or acquired, arising from prior intervention (e.g., adult congenital heart disease), drug-related toxicities (e.g., SOS) or from idiopathic thrombotic events (Budd-Chiari syndrome). In some cases, these may result in the formation of benign lesions which can be challenging to differentiate from malignancy.

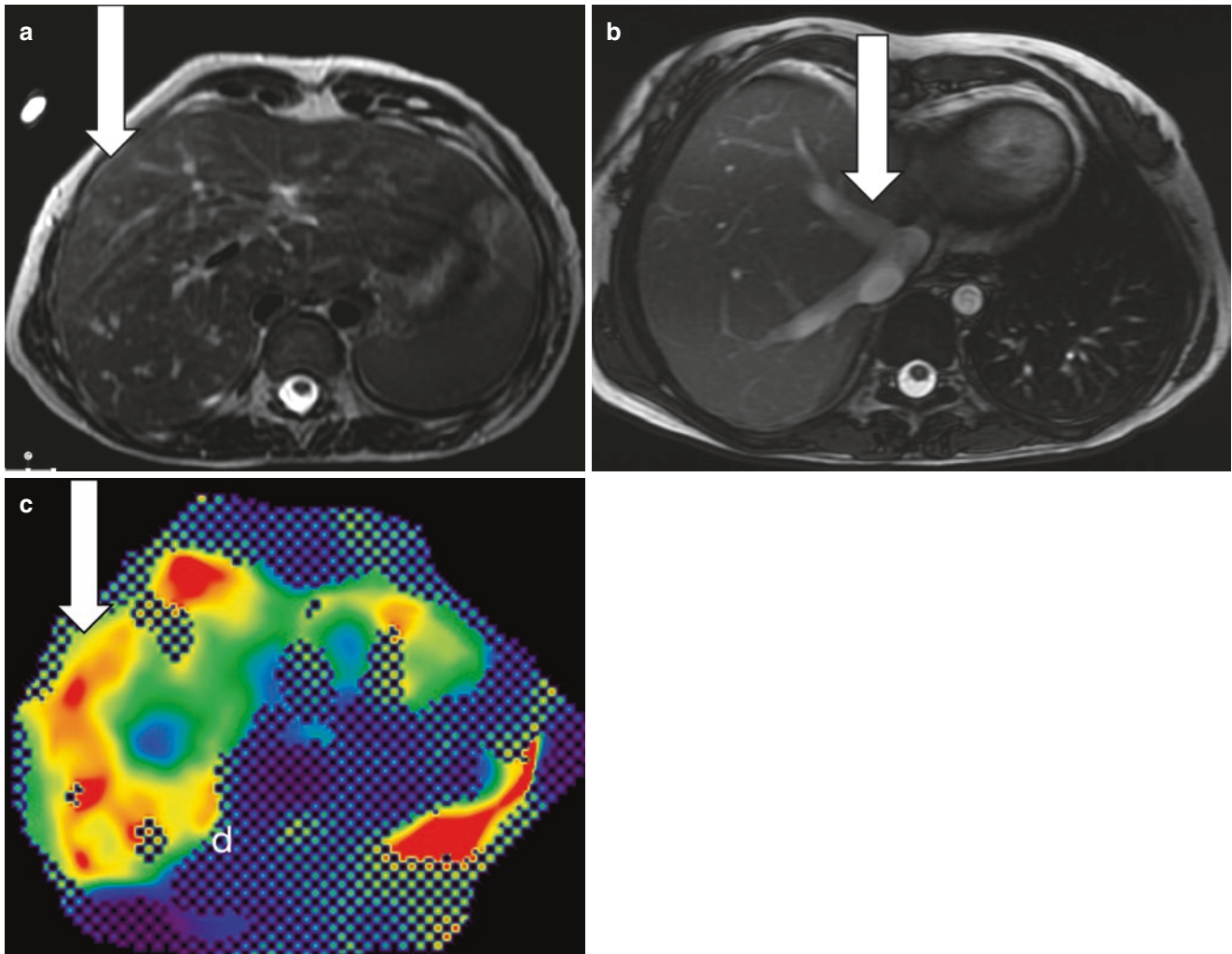


Fig. 6.10 Fontan-associated liver disease in a young adult patient 20 years following corrective surgery. (a) Axial T2-weighted image shows diffuse peripheral T2 hyperintensity (arrow), with dilated hepatic veins (b) in keeping with hepatic congestion. (c) Color MR elastogram

demonstrates elevated stiffness within the periphery, supportive of congestion as the predominant pathology. Ultimately, there will be progression to fibrosis and cirrhosis in the absence of effective treatment

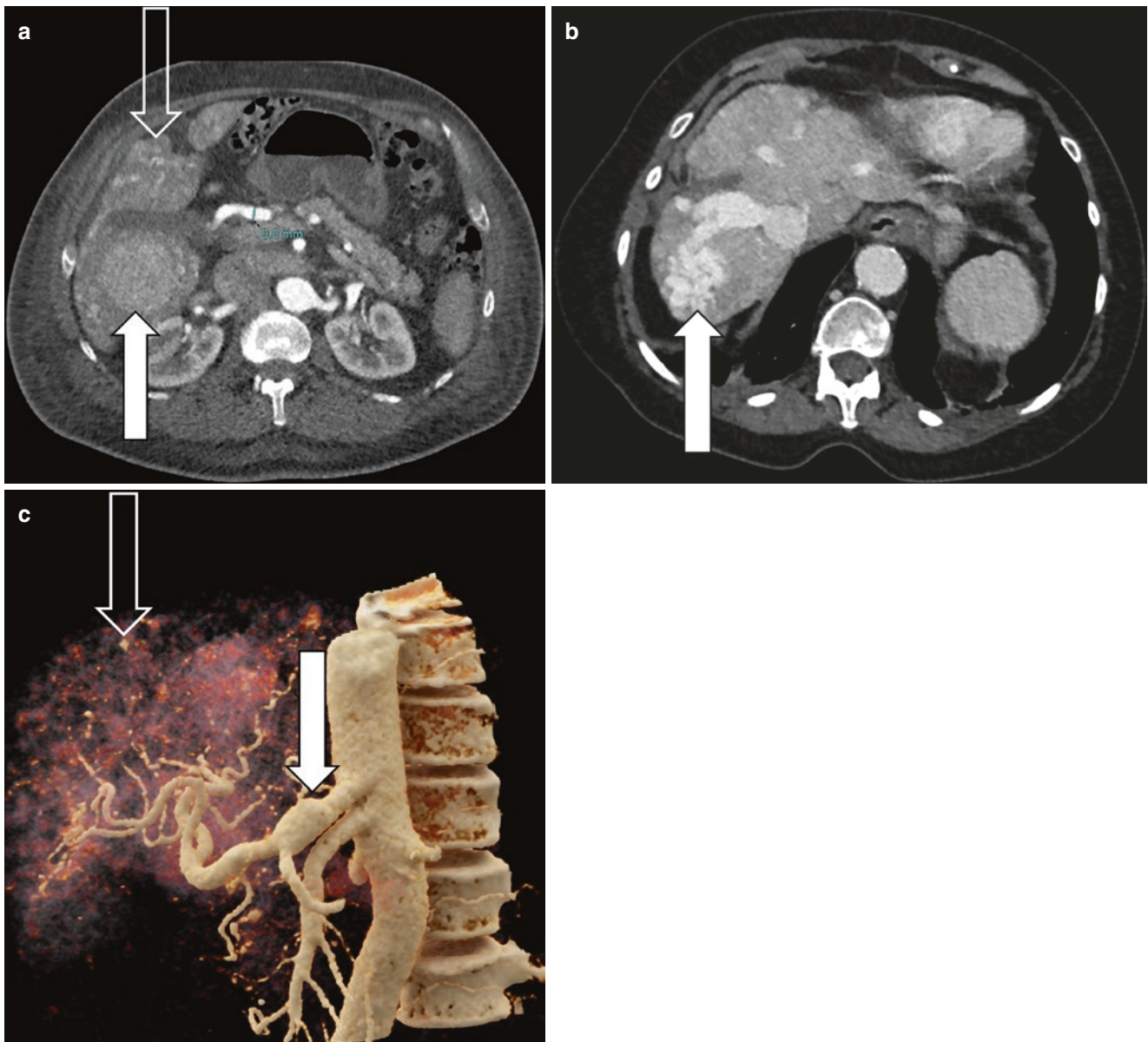


Fig. 6.11 Vascular findings in a patient with hereditary hemorrhagic telangiectasia. (a) Axial arterial phase CT image demonstrating dilatation of the common hepatic artery (9 mm), a large confluent vascular mass (white arrow) and multiple tiny telangiectasias (open arrow). (b) Axial portal venous phase CT image showing large portal to hepatic

venous shunts, with resultant dilatation of the right hepatic vein. (c) Volume-rendered image of the same patient, demonstrating aneurysmal dilatation of the celiac axis (white arrow), a large caliber common hepatic artery and multiple tiny hepatic telangiectasias (open arrow)

6.5 Diffuse Metastatic Disease

Hepatic metastases may show an infiltrative growth pattern with intrasinusoidal spread of tumor cells, which has been reported in breast cancer, gastric cancer, urothelial, small cell lung cancer, and melanoma. The intrasinusoidal spread induces hepatic ischemia, necrosis, and tumoral portal vein thrombosis leading to acute liver failure. Imaging diagnosis is difficult as no typically focal liver metastases can be seen.

The diffusely infiltrated liver parenchyma can appear heterogeneous compared to normal parenchyma. MRI is helpful to identify diffuse metastatic spread showing marked hyperintensity on diffusion-weighted images and hypointensity on hepatobiliary phase images. The degree of enhancement is variable also depending on the underlying primary tumor. Definite diagnosis can only be made by biopsy.

Another rare type of diffuse liver parenchyma changes is the so-called pseudocirrhosis, which can appear with hepatic

breast cancer metastases and less common in cancer of the gastrointestinal tract, ovarian, or thyroid cancer [26]. The liver shows a nodular contour, capsular retraction, and shrinkage. Even signs of portal hypertension can develop over time. The etiology of the pseudocirrhosis is not very clear; it can be seen after chemotherapy with capsular retractions at the site of the liver metastases as response to chemotherapy, but it can also result from desmoplastic reaction surrounding the liver metastases.

6.6 Concluding Remarks

Chronic liver disease, in particular cirrhosis, is an increasing global epidemic which has already resulted in a major burden on healthcare systems with an ever-increasing incidence of primary liver malignancies and hepatic decompensation. Early identification of those at risk using quantitative imaging techniques, in particular elastography, fat fraction assessment and iron quantification is therefore essential in order to reduce its impact. MR elastography has proven a robust and accurate methodology for the assessment of those in whom rapid clinic-based techniques are unreliable. While outside the scope of this review, future developments of this technology (e.g., 3D MRE) may provide additional valuable information that could, for example, enable the differentiation of fibrosis from congestion in patients with vascular disorders such as congestive heart failure. When assessing those with cirrhosis, a methodical and consistent approach is required in order to identify malignancies, and in particular HCC, at a sufficiently early stage to enable effective treatment.

Take Home Messages

- Metabolic disease and cirrhosis are frequently under-recognized.
- Familiarity with the morphologic features of diffuse liver disease and current/emerging quantitative imaging techniques is key to its early identification.
- A consistent, rigorous approach to the assessment of associated lesions (e.g., using the LiRADS system) is essential and aids communication between clinicians as well as improving consistency in reporting.
- Vascular liver disease may lead to chronic liver damage and development of regenerative nodules, which need to be differentiated from HCC.

References

1. Sepanlou, et al. The global, regional, and national burden of cirrhosis by cause in 195 countries and territories, 1990–2017: a systematic analysis for the Global Burden of Disease Study 2017. *Lancet Gastroenterol Hepatol.* 5:245–66. [https://doi.org/10.1016/S2468-1253\(19\)30349-8](https://doi.org/10.1016/S2468-1253(19)30349-8).
2. Pickhardt PJ, et al. Specificity of unenhanced CT for non-invasive diagnosis of hepatic steatosis: implications for the investigation of the natural history of incidental steatosis. *Eur Radiol.* 2012;22(5):1075–82. <https://doi.org/10.1007/s00330-011-2349-2>. Epub 2011 Dec 4.
3. Idilman IS, Aniktar H, Idilman R, et al. Hepatic steatosis: quantification by proton density fat fraction with MR imaging versus liver biopsy. *Radiology.* 2013;267(3):767–75.
4. Hernando D, Levin YS, Sirlin CB, Reeder SB. Quantification of liver iron with MRI: state of the art and remaining challenges. *J Magn Reson Imaging.* 2014 Nov;40(5):1003–21. <https://doi.org/10.1002/jmri.24584>.
5. Henninger B, et al. Performance of different Dixon-based methods for MR liver iron assessment in comparison to a biopsy-validated R2* relaxometry method. *Eur Radiol.* 2021;31(4):2252–62.
6. Akhan O, et al. Imaging findings of liver involvement of Wilson's disease. *Eur J Radiol.* 2009;69(1):147–55.
7. Venkatesh SK, Hoodeshenas S, Venkatesh SH, Dispenzieri A, Gertz MA, Torbenson MS, Ehman RL. Magnetic resonance elastography of liver in light chain amyloidosis. *J Clin Med.* 2019;8(5):739.
8. Regenboog M, et al. Hepatocellular carcinoma in Gaucher disease: an international case series. *J Inher Metab Dis.* 2018;41(5):819–27.
9. Guglielmo FF, Venkatesh SK, Mitchell DG. Liver MR elastography technique and image interpretation: pearls and pitfalls. *Radiographics.* 2019;39(7):1983–2002.
10. Yin M, Glaser KJ, Talwalkar JA, Chen J, Manduca A, Ehman RL. Hepatic MR elastography: clinical performance in a series of 1377 consecutive examinations. *Radiology.* 2016;278(1):114–24.
11. Brancatelli G, Federle MP, Ambrosini R, et al. Cirrhosis: CT and MR imaging evaluation. *Eur J Radiol.* 2007;61(1):57–69.
12. Parente DB, Perez RM, Eiras-Araujo A, et al. MR imaging of hypervascular lesions in the cirrhotic liver: a diagnostic dilemma. *Radiographics.* 2012;32(3):767–87.
13. LeGout JD, Bolan CW, Bowman AW, Caserta MP, Chen FK, Cox KL, Sanyal R, Toskich BB, Lewis JT, Alexander LF. Focal nodular hyperplasia and focal nodular hyperplasia-like lesions. *Radiographics.* 2022;42(4):1043–61.
14. Suh CH, et al. Hypervascular transformation of hypovascular hypointense nodules in the hepatobiliary phase of gadoteric acid-enhanced MRI: a systematic review and meta-analysis. *AJR Am J Roentgenol.* 2017;209(4):781–9.
15. McEvoy SH, et al. Hepatocellular carcinoma: illustrated guide to systematic radiologic diagnosis and staging according to guidelines of the American Association for the Study of Liver Diseases. *Radiographics.* 2013;33(6):1653–68.
16. Razumilava N, Gores GJ. Cholangiocarcinoma. *Lancet.* 2014;383(9935):2168–79.
17. Kim R, et al. Differentiation of intrahepatic mass-forming cholangiocarcinoma from hepatocellular carcinoma on gadoteric acid-enhanced liver MR imaging. *Eur Radiol.* 2016;26(6):1808–17.
18. Reynolds AR, et al. Infiltrative hepatocellular carcinoma: what radiologists need to know. *Radiographics.* 2015;35(2):371–86.
19. Ronot M, et al. Focal lesions in cirrhosis: not always HCC. *Eur J Radiol.* 2017;93:157–68.

20. <https://www.acr.org/Clinical-Resources/Reporting-and-Data-Systems/LI-RADS>
21. Torabi M, Hosseinzadeh K, Federle MP. CT of nonneoplastic hepatic vascular and perfusion disorders. *Radiographics*. 2008;28(7):1967–82.
22. Shin NY, et al. Accuracy of gadoxetic acid-enhanced magnetic resonance imaging for the diagnosis of sinusoidal obstruction syndrome in patients with chemotherapy-treated colorectal liver metastases. *Eur Radiol*. 2012;22(4):864–71.
23. Elsayes KM, et al. A comprehensive approach to hepatic vascular disease. *Radiographics*. 2017;37(3):813–36.
24. Idilman IS, Li J, Yin M, Venkatesh SK. MR elastography of liver: current status and future perspectives. *Abdom Radiol (NY)*. 2020;45(11):3444–62.
25. Buscarini E, Gandolfi S, Alicante S, Londoni C, Manfredi G. Liver involvement in hereditary hemorrhagic telangiectasia. *Abdom Radiol (NY)*. 2018;43(8):1920–30.
26. Gopalakrishnan D, et al. Pseudocirrhosis in breast cancer—experience from an Academic Cancer Center. *Front Oncol*. 2021;11:679163.

Open Access This chapter is licensed under the terms of the Creative Commons Attribution 4.0 International License (<http://creativecommons.org/licenses/by/4.0/>), which permits use, sharing, adaptation, distribution and reproduction in any medium or format, as long as you give appropriate credit to the original author(s) and the source, provide a link to the Creative Commons license and indicate if changes were made.

The images or other third party material in this chapter are included in the chapter's Creative Commons license, unless indicated otherwise in a credit line to the material. If material is not included in the chapter's Creative Commons license and your intended use is not permitted by statutory regulation or exceeds the permitted use, you will need to obtain permission directly from the copyright holder.

